J. Fluid Mech. (1988), *vol.* 191, *pp.* 197–223
Printed in Great Britain

Flow structure from an oscillating cylinder Part 1. Mechanisms of phase shift and recovery in the near wake

By A. ONGOREN AND D. ROCKWELL

Department of Mechanical Engineering and Mechanics, Lehigh University, Bethlehem, PA 18015, USA

(Received 10 July 1986 and in revised form 1 September 1987)

Cylinders of various cross-section were subjected to controlled oscillations in a direction transverse to the incident flow. Excitation was at frequency f_e, relative to the formation frequency f_0^* of large-scale vortices from the corresponding stationary cylinder, and at Reynolds numbers in the range $584 \leqslant Re \leqslant 1300$. Modifications of the near wake were characterized by visualization of the instantaneous flow structure in conjunction with body displacement–flow velocity correlations.

At $f_e/f_0^* = \frac{1}{2}$, corresponding to subharmonic excitation, as well as at $f_e/f_0^* = 1$, the near wake structure is phase-locked (synchronized) to the cylinder motion. However, the synchronization mechanism is distinctly different in these two regimes. Near or at $f_e/f_0^* = 1$, the phase of the shed vortex with respect to the cylinder displacement switches by approximately π. Characteristics of this phase switch are related to cylinder geometry. It does not occur if the cylinder has significant afterbody.

Over a wide range of f_e/f_0^*, the perturbed near wake rapidly recovers to a large-scale antisymmetrical mode similar in form to the well-known Kármán vortex street. The mechanisms of small-scale (f_e) vortex interaction leading to recovery of the large-scale (f_0) vortices are highly ordered and repeatable, though distinctly different, for superharmonic excitation ($f_e/f_0^* = n = 2, 3, 4$) and non-harmonic excitation (non-integer values of f_e/f_0^*).

The frequency f_0 of the recovered vortex street downstream of the body shows substantial departure from the shedding frequency f_0^* from the corresponding stationary body. It locks-on to resonant modes corresponding to $f_0/f_e = 1/n$. This wake response involves strictly hydrodynamic phenomena. It shows, however, a resonant behaviour analogous to that of coupled flow–acoustic systems where the shear layer is convectively unstable

1. Introduction

Flow-induced loading and vibration of a cylinder in crossflow have been investigated from a variety of perspectives during the past few decades. Recent advances in our understanding of this class of flow–structure interaction are summarized in the insightful overviews of Mair & Maull (1971), Berger & Wille (1972), Parkinson (1974), Sarpkaya (1979), Bearman & Graham (1980), and Bearman (1984).

A number of advances have been made in the past two decades relating the visualized flow structure downstream of the body to the frequency of oscillation of the body; typically, the oscillation frequency of the body is at or near the inherent

vortex-shedding frequency from the corresponding stationary body. Koopmann (1967*a*, *b*), Griffin & Votaw (1972), and Griffin (1971, 1973) have contributed substantially to our understanding of the alteration of the near-wake structure for excitation conditions at or near synchronization. Moreover, the reviews of Berger & Wille (1972), Sarpkaya (1979) and Mair & Maull (1971) provide assessments of various features of the near-wake characteristics.

Of the many investigations in recent years, we first focus on those that characterize the transverse force, or surface pressure, in the range where the excitation frequency f_e is close to, or the same as the natural shedding frequency f_0^* when the body is stationary, i.e. $f_e/f_0^* \sim 1$. Bishop & Hassan (1964) and Staubli (1981) have revealed a sudden change in the phase angle between the transverse force F_y and cylinder displacement Y in this range; moreover, Sarpkaya (1978) demonstrated that there are correspondingly strong variations of the in-phase and out-of-phase force coefficients. Another means of characterizing the loading on the cylinder is measurement of the fluctuating pressure on the side of the cylinder. For the case of forced oscillations, studies by Bearman & Currie (1979), as well as for free oscillations, examined by Feng (1968) and Ferguson & Parkinson (1967), there are drastic changes in phase angle of the fluctuating pressure relative to the cylinder displacement through the synchronization range. Moreover, these severe changes in loading are not limited to the configuration of the circular cylinder. Bearman & Obasaju (1982) reveal a sharp variation in phase angle between pressure measured on the centre of the side face of a rectangular cylinder and its displacement; however, this phase shift occurred at a Strouhal number substantially lower than those of the aforementioned cases of the circular cylinder.

In contrast to these well-studied features of the cylinder loading, relatively little is known of the corresponding flow structure in the near-wake region. On the basis of the foregoing studies, it is clear that there is some sort of sudden shift in the near-wake dynamics within the $f_e/f_0^* \sim 1$ range; however, its precise nature remains unresolved. An important observation in this direction has been made by Zdravkovich (1982). From study of flow-visualization films of Den Hartog (1934), Meier-Windhorst (1939) and Angrilli, DiSilvio & Zanardo (1974), encompassing both free and forced oscillations, he suggests that the drastic changes in phase of the loading described in the foregoing are due to corresponding changes in the phasing of the vortex shedding with respect to displacement of the cylinder. In essence, in passing from flow conditions below the range $f_e/f_0^* \sim 1$ to above it, the phase angle between the initially shed vortex and cylinder displacement changes by the order of π.

Among the unresolved issues related to alteration of the flow structure through this range are: the underlying physical mechanism(s) for a possible phase shift of the vortex shedding (relative to the displacement of the cylinder) through the synchronization range, including the relation between this phasing and the vortex formation length; quantitative characterization of the phase shift of the shed vortices as a function of excitation frequency in the near-wake region, thereby determining to what degree this phase shift is 'discontinuous', as opposed to a more gradual transition between modes of shedding; and effect of cylinder base geometry on the near-wake structure, especially the influence of afterbody length (i.e. portion of body downstream of separation points) on the mechanism of phase shift. Although there is a tendency to focus on regimes of excitation within and near $f_e/f_0^* \sim 1$ when examining these types of problems, there is much to be learned by considering excitation frequencies below and above this range. In this regard, a primary issue is

determining the possibility of phase shift of the vortex-shedding process at frequencies well below and above $f_e/f_0^* \sim 1$. Such a study might provide insight into the flow mechanisms occurring within the synchronization region itself.

Moreover, excitation of the cylinder at frequencies well away from the natural shedding frequency ($f_e/f_0^* = 1$) is expected to induce vortical structures in the near wake at f_e. The following issue arises. Is there rapid recovery of the flow structure to the large-scale antisymmetrical mode of f_0? If so, what is the nature of the vortex–vortex interactions leading to 'recovery' of the mode at f_0, and is the frequency f_0 itself somehow related to a dimensionless form of f_e? These aspects must, of course, be assessed relative to extensively investigated instabilities of jets and mixing layers. The likelihood of an absolute instability of a bluff-body wake (Monkewitz & Nguyen 1986), as opposed to the convective instability of typical jets and mixing-layers (Ho & Huerre 1984), is expected to exert a predominant influence on the near-wake structure.

In this investigation, we address these unresolved issues by subjecting cylinders to controlled oscillations at defined frequency and amplitude, while characterizing the flow structure in the near-wake region. We first examine the concept of synchronization, i.e. phase-locking, of the vortex formation with respect to the body motion. Then, for conditions at which synchronization occurs, we address the phase shift of the vortex formation with respect to the body motion. Finally, attention is focused on the manner in which the highly distorted near wake at f_e evolves into the classical Kármán mode at f_0. In doing so, wakes from cylinders having oscillating versus fixed separation points and zero versus finite afterbody are addressed in order to determine the common and distinguishing consequences of these parameters.

2. Experimental system and instrumentation

As described in detail by Ongoren (1986), the cylinder was mounted vertically in a free-surface water channel, with its bottom end free and its top end clamped to the driving mechanism. Three basic cylinder configurations were employed in this study: circular; triangular; and rectangular. Denoting the transverse (projected) dimensions of each cylinder as D, each has a value of $D = 1.27$ cm and a length of $L = 36.3$ cm. The cylinder and its mounting arrangement were sufficiently rigid to preclude deflection during forced oscillations. Moreover, it was necessary to ensure that its metallic surface was well insulated from the electrolysis process during hydrogen-bubble visualization. These two demands of stiffness and insulation were met by fabricating the cylinders from two concentric cylinders, the outer cylinder of Plexiglas having inner and outer radii of 6.35 mm and 12.7 mm, and the inner cylinder of steel having a radius of 6.35 mm. Similar techniques were employed in fabrication of the triangular- and square-cross-section cylinders.

During preliminary experiments, considerable effort was expended in ensuring that free-surface dynamics did not influence the near-wake dynamics. To achieve this, a special cover plate, extending $12D$ upstream and $36D$ downstream of the centreline of the cylinder was designed. Another possible influence is the existence of resonant frequencies of the excitation system itself, i.e. the motor–pulley–bearing arrangement. Such disturbances propagate to the cylinder and induce small-scale instabilities in the near-wake region. This problem was finally circumvented by several successive designs of the system.

Most experiments were carried out at a Reynolds number $Re = 855$, though the basic flow structure described herein was observed up to $Re = 3000$, the upper limit

of the experimental arrangement. The oscillation amplitude of the cylinder was maintained at $Y_e/D = 0.13$ for all values of Reynolds number. Several criteria were satisfied in the selection of $Re = 855$ as the primary one. First, to make interpretation of the near-wake dynamics as simple as possible, it was desired to have a single predominant frequency and purely antisymmetrical growth of the large-scale instability in the near-wake region. These criteria were ascertained by cross-spectral measurements between hot-film probes mounted on either side of the wake. At higher values of the Reynolds number than that selected here, small-scale 'transition waves', riding upon the large-scale vortices, were observed; they were similar to those noted by Unal & Rockwell (1988), as well as in previous studies of Gerrard (1978) and Wei & Smith (1986). Another consideration in selection of the Reynolds number is the flow-visualization technique; hydrogen bubbles accurately track the flow-field unsteadiness only if the velocity is sufficiently high (Schraub *et al.* 1965). On the other hand, the velocity must be sufficiently low to provide sufficiently high contrast of the bubble timelines during photography.

At $Re = 855$, the Strouhal number of vortex shedding was $f_0^* D/U = 0.194$, 0.200 and 0.135, for the circular, triangular, and square cross-sections respectively. For all cylinders, D represents the diameter or width in the cross-stream direction, f_0^* the frequency of vortex formation from the stationary body, and U the free-stream velocity. The ratio f_e/f_0^* employed extensively in this investigation therefore represents the ratio of Strouhal numbers at the forced and self-excited frequencies.

As shown in Ongoren (1986), the 1 mm platinum wire used for generating hydrogen bubbles was oriented with its axis in the horizontal plane at a location $0.4D$ upstream of the cylinder centreline, supported by two prongs $24D$ apart. For certain types of visualization, the central portion of the wire was coated with liquid insulator, allowing detailed observation of the forward stagnation region of the cylinder, as well as the local separation region. The visualized timelines were recorded on an Instar television system having a frame rate of 120 frames per s. Moreover, using the split-screen capability in conjunction with a second camera, it was possible to record simultaneously: the cylinder displacement trace as observed on a storage oscilloscope; the oscillating cylinder; and the visualized timeline pattern of the near wake.

The phase of the vortex-shedding process, relative to the displacement of the cylinder, was quantitatively determined by cross-spectral analysis between: a hot-film located at the outer edge of the downstream wake; and a signal from the displacement transducer mounted on the cylinder mechanism. The transverse location of the hot film is crucial, since it is well known that there are strong transverse gradients of the phase of the fluctuating velocity field, a principle well established through linear stability analysis (Michalke 1965). Consequently, it is necessary to take preliminary phase measurements in the transverse direction to ensure that the hot film is located in a region of minimum phase gradient. This condition is satisfied just beyond the outer edge of the mean shear layer from the cylinder.

3. Synchronization of vortex formation

We first address the conditions for which the near-wake structure is phase-locked, i.e. synchronized, with the cylinder motion. The phase of the vortex formation was tracked for several excitation frequencies in the range $0 \leqslant f_e/f_0^* \leqslant 1$, as indicated in figure 1. Only the cylinder frequency f_e was varied to give different values of f_e/f_0^*.

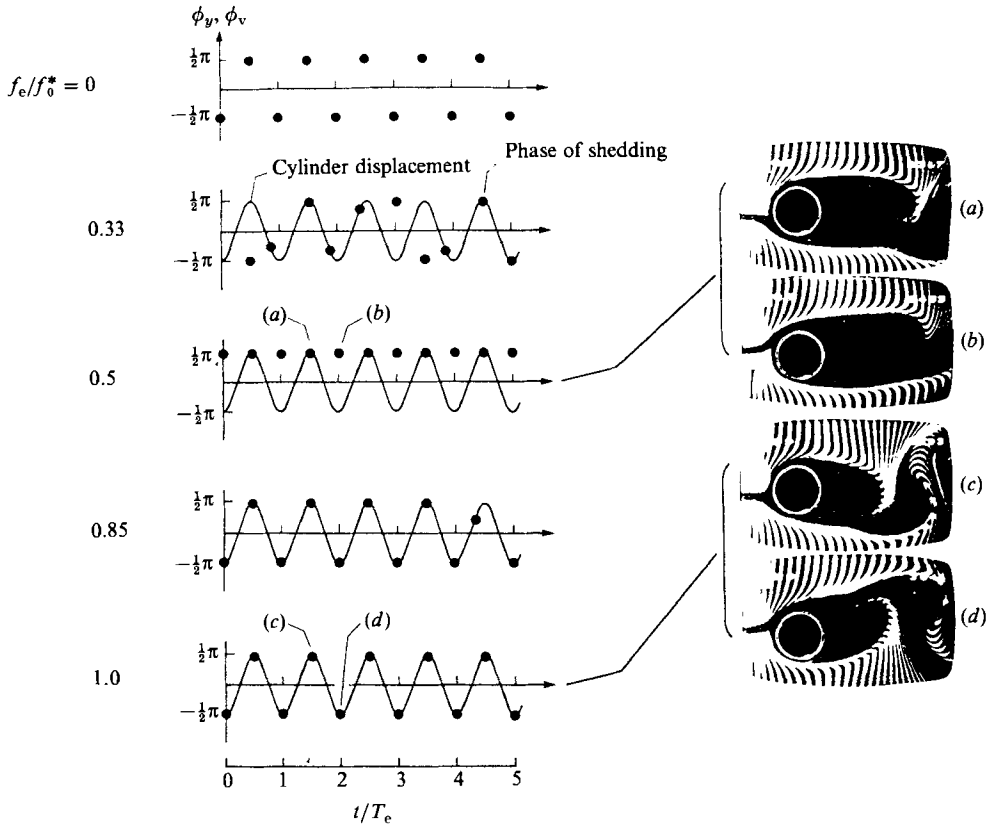

FIGURE 1. Phase of vortex shedding ϕ_v (dots) relative to phase of cylinder displacement ϕ_y as function of time for excitation frequencies $f_e/f_0^* = 0$, 0.33, 0.50, 0.85 and 1.0.

Note that the time t is normalized by the period $T_e \equiv 1/f_e$, which varies in accord with f_e. Therefore, the spacing on the t/T_e axis is the same for all values of T_e. For $f_e/f_0^* = 0$, there is no body motion; vortices are shed alternately with increasing time. At $f_e/f_0^* = 0.33$, the solid line shows the sinusoidal cylinder displacement and the solid dots represent the occurrence of vortex formation, corresponding to drawing of irrotational fluid across the wake centreline. In this case the modulation in the phase of vortex shedding is indeed substantial. Although this phase, relative to the body motion, is modulated, it should be emphasized that the vortex formation retains its antisymmetrical, harmonic behaviour.

At $f_e/f_0^* = \frac{1}{2}$, there is subharmonic synchronization; the initial vortex shedding is phase-locked such that it is alternately in phase (i.e. $\Delta\phi_v = 0$), then out-of-phase (i.e. $\Delta\phi_v = \pi$) with the body motion. Although two vortices are shed for every period of cylinder displacement, the initial vortex consistently forms on the same side (upper side) of the cylinder irrespective of whether the displacement is either maximum negative or positive. These features of the vortex formation are displayed in photos (*a*) and (*b*) in figure 1. In photo (*a*), the cylinder is at its maximum positive position ($Y = Y_e$), and in photo (*b*) it is at maximum negative position ($Y = -Y_e$). In both photos, however, vortex formation is consistently from the upper side of the cylinder.

Two higher frequencies, $f_e/f_0^* = 0.85$ and $f_e/f_0^* = 1$, are also included in this series

of plots to illustrate the approach to synchronization at the fundamental frequency of vortex formation; it is the classical type of synchronization. At $f_e/f_0^* = 0.85$, the vortex shedding is essentially synchronized. Loss of phase-locking occurs only every ten cycles or so; for $f_e/f_0^* = 1$, there is complete synchronization. Photos (*c*) and (*d*) in figure 1 show complete synchronization at $f_e/f_0^* = 1$; in photo (*c*), the initial vortex is on the upper side and the cylinder displacement is positive maximum; in photo (*d*) the cylinder displacement is negative maximum and the initial vortex appears on the lower side.

We emphasize that the synchronization characteristics defined here hold only for the considered oscillation amplitude. At higher amplitudes, the extent of the synchronization range should increase; at the other extreme, i.e. at a sufficiently small amplitude, the synchronization range may cease to exist altogether. This aspect remains for investigation.

In the foregoing, we have addressed the conditions for which the vortex shedding is locked to the cylinder motion. Within this lock-in range, however, the phase of the actual vortex formation with respect to the body motion may vary as a function of forcing frequency. We now turn to this aspect.

4. Phase shift of vortex formation

4.1. *Overview of vortex formation relative to cylinder displacement: circular cylinder*

Figure 2 gives an overview of the near-wake structure of a cylinder over a frequency range $0.85 \leqslant f_e/f_0^* \leqslant 1.17$. To allow comparison of the phasing of the initially shed vortex relative to the instantaneous displacement of the cylinder, all photos in figure 2 are at the instant of maximum negative displacement of the cylinder, $Y = -Y_e$. The portion of the bubble wire intersecting the $Y = 0$ axis of the stationary cylinder was insulated to provide insight into the fluctuation of the forward stagnation region.

Comparison of photos corresponding to $f_e/f_0^* = 0.85$, 0.9, and 1 shows that there is substantial decrease in vortex formation length and simultaneously an increase in angle of inclination of the base region, which we designate as α_w. In the photo corresponding to $f_e/f_0^* = 1.05$, there is a tendency towards initial vortex shedding from the upper, as opposed to the lower, side of the cylinder; in the photo corresponding to $f_e/f_0^* = 1.17$, this switch in phase of the initially shed vortex is completed. Correspondingly, there is no longer a perceptible inclination of the base region, i.e. $\alpha_w \approx 0$. In summary, as suggested in figure 2, and described in detail by Ongoren (1986), as the frequency ratio $f_e/f_0^* \sim 1$ is approached, there is substantial shortening of the vortex formation length and increase in angle of inclination α_w of the base region. However, just above this frequency ratio, there is a switch in phase of the vortex shedding to the opposite side of the cylinder in conjunction with a decrease in the inclination angle α_w of the base region to approximately zero.

Moreover, as addressed by Ongoren (1986), the variations of angle α_w and phase shift of the vortex formation are remarkably well correlated with previous observations of the lift amplitude and phase respectively.

4.2. *Overview of vortex formation relative to cylinder displacement: triangular-cross-section cylinder*

Figure 3 shows the near-wake structure of the triangular-cross-section cylinder. As in figure 2, all photos correspond to the maximum negative location of the cylinder

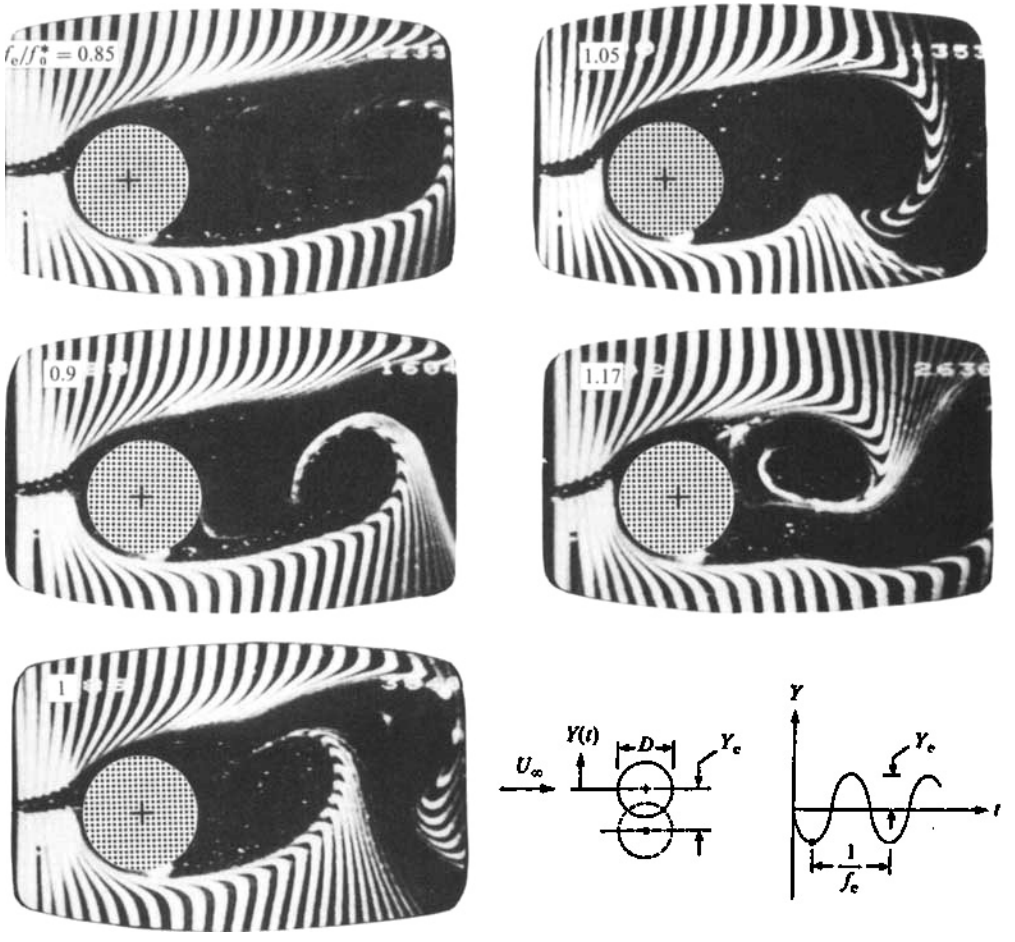

FIGURE 2. Effect of ratio of excitation frequency f_e to natural shedding frequency f_0^* on near-wake structure. All photos taken at maximum negative displacement of cylinder.

$Y = -Y_e$. At a frequency ratio $f_e/f_0^* = 0.9$, relative to $f_e/f_0^* = 0.8$, there is a substantial decrease in vortex formation length. In fact, the vortex forms immediately behind the cylinder. Furthermore, comparing photos representing frequency ratios $f_e/f_0^* = 0.9$ and 1, there is clearly a phase shift of approximately π of the initial vortex formation relative to the body motion. Increasing the frequency ratio f_e/f_0^* to a much higher value, $f_e/f_0^* = 2$, causes the near-wake region to break into small-scale vortex formation; subsequently, the small-scale vortices interact with one another, especially evident in the top row of vortices in these photos. This drastic change in the near-wake structure clearly prolongs the distance over which the classical large-scale vortices form. There is no sweeping of irrotational fluid across the wake centreline due to large-scale vortex formation, at least within the flow domain illustrated in the last two photos in the right column.

Considering the photo series of figure 3 as a whole, it is evident that the phenomenon of 'wake swing', or inclination of the base angle α, observed for the circular cylinder (figure 2) is not present. Therefore, we conclude that the mechanism leading to the phase shift of the vortex shedding with respect to the body motion does not require fluctuation of the separation points, which is directly linked to base

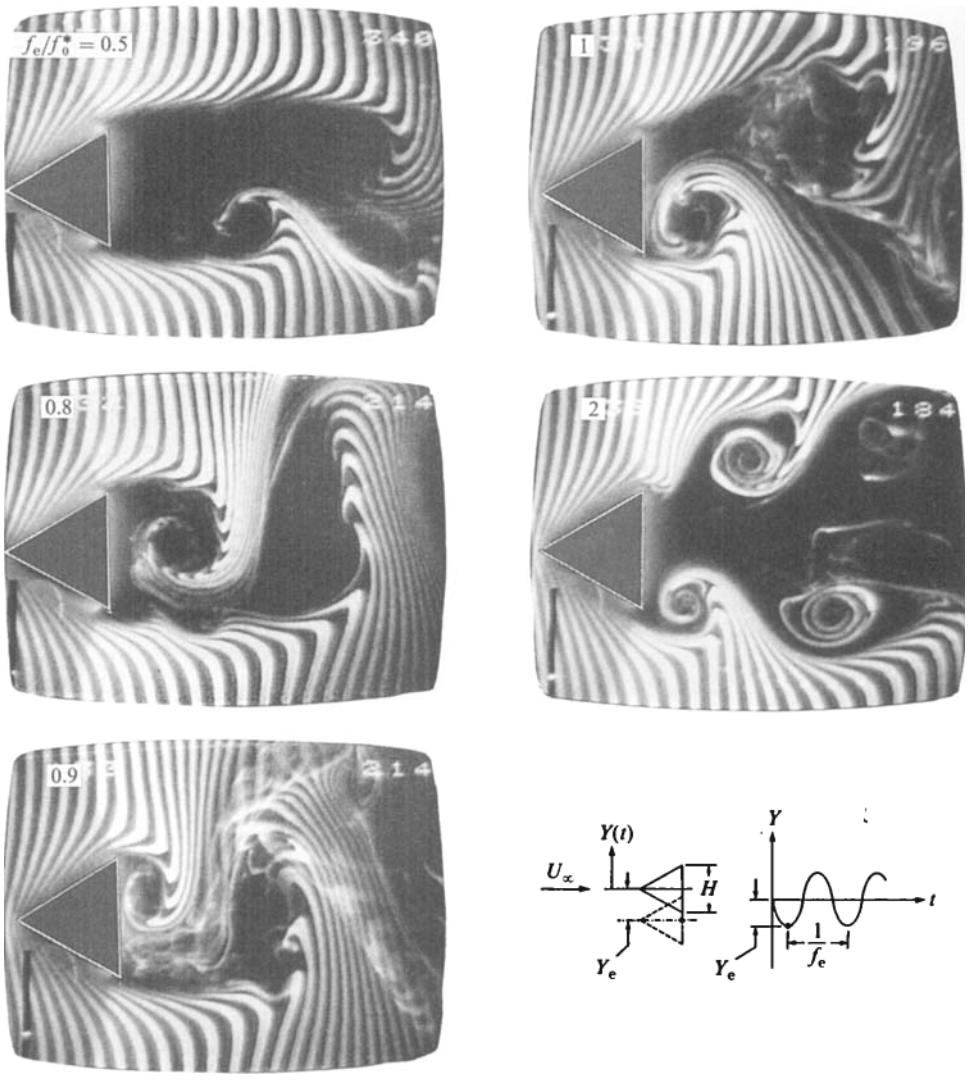

FIGURE 3. Near-wake of oscillating cylinder having triangular cross-section as function of frequency ratio f_e/f_0^*. All photos taken at maximum negative displacement of cylinder.

angle inclination α_w. Rather, it is primarily due to the attainment of minimum vortex formation length. Indeed, this occurrence of minimum formation length with increasing f_e/f_0^* is a strikingly common feature of the near-wake structure of the circular and triangular cylinders (figures 2 and 3). An interesting difference, however, is the direction of the phase switch of the vortex shedding in passing through $f_e/f_0^* \approx 1$. Comparing the photos corresponding to $f_e/f_0^* = 0.9$ and 1 of figure 3 and the photos corresponding to $f_e/f_0^* = 1$ and 1.17 of figure 2, it is evident that the phase switch occurs in different directions for the circular and triangular cylinders; that is, for $f_e/f_0^* < 1$, the first vortex is formed on the lower side of the circular cylinder, and on the upper side of the triangular cylinder; the converse holds for $f_e/f_0 > 1$.

Complete time sequences of the shedding process are given by Ongoren (1986) for

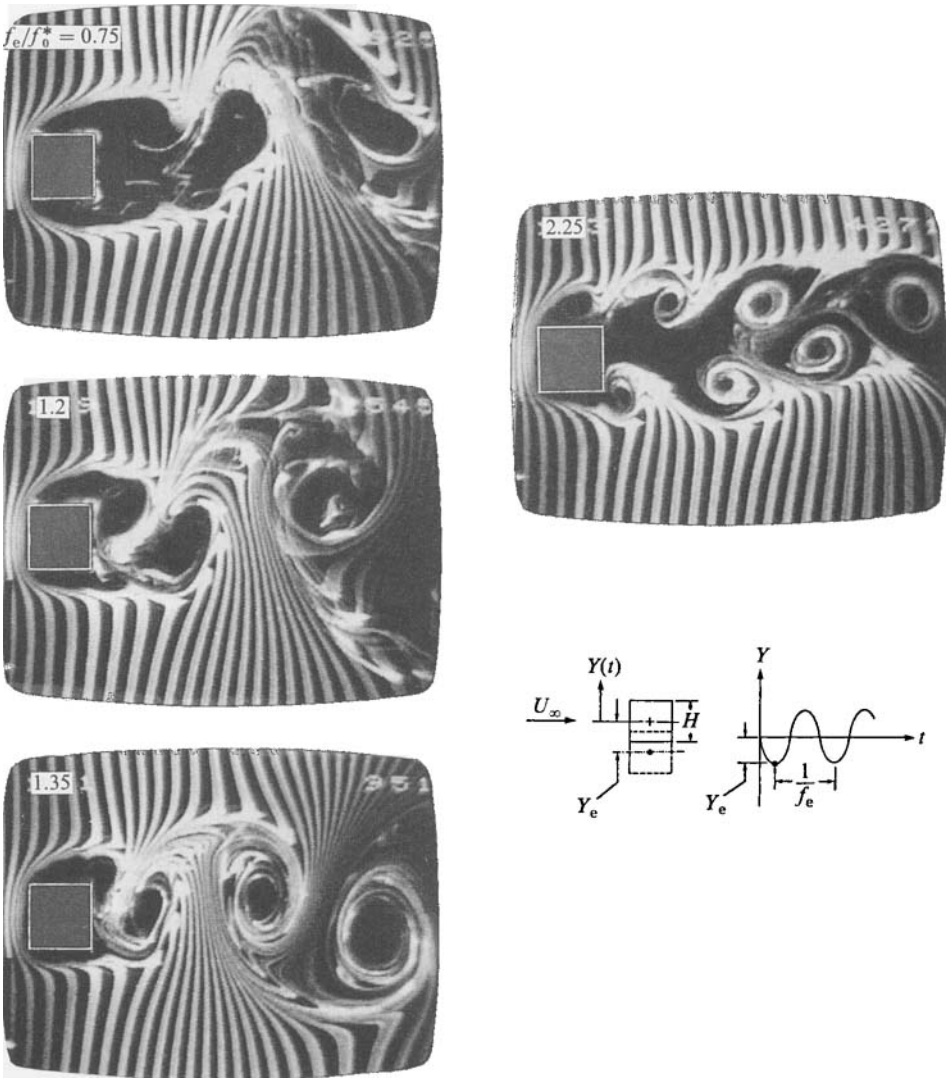

FIGURE 4. Near-wake of square-cross-section cylinder as function of frequency ratio f_e/f_0^*. All photos taken at instant corresponding to maximum negative displacement of cylinder.

both triangular- and circular-cross-section cylinders. By comparing corresponding photographs at the same instant during the oscillation cycle, it is evident that the shedding process is always out-of-phase by approximately π.

4.3. *Overview of vortex formation relative to cylinder displacement: square-cross-section cylinder*

For the square-cross-section cylinder (figure 4), the flow structure of the near wake and the character of the phase shift downstream of the cylinder is dramatically different than the aforementioned cases. As in previous cases, all photos are taken at the maximum negative position of the cylinder, $Y = -Y_e$ during a typical oscillation cycle. Study of, for example, the separating shear layer on the upper side of the rectangular cylinder shows that, in the photos corresponding to frequency ratios

0.75–2.25 successively, the vortex formation length decreases until there is instantaneous reattachment to the trailing end of the cylinder, evident at $f_e/f_0^* = 1.2$. (At higher values of f_e/f_0^* (not shown), this reattachment moves to, then upstream of, the trailing corner of the cylinder.) Correspondingly, at successively higher f_e/f_0^*, there is upstream migration of the first vortex of counter-clockwise sense to the base of the cylinder. This process is evident in the photos corresponding to $f_e/f_0^* = 0.75$, 1.2 and 1.35. It eventually breaks away from the base region in favour of small-scale vortices, as shown in the photos for $f_e/f_0^* = 2.25$. Corresponding to this sudden change in the flow pattern is a marked decrease in the wavelength between vortices on either side of the near-wake region.

The most remarkable feature, however, of the vortex formation from this square cross-section is that the phasing of the vortex shedding relative to the body motion does not undergo the type of switching in the range $f_e/f_0^* = 1$, as was previously described for the circular and triangular cross-sections. Considering the flow patterns shown for $f_e/f_0^* = 0.75$ and 1.2, there is no change in timing of the vortex shedding, but simply a shortening of the vortex formation length.

Moreover, we note that excitation of the separating shear layers leading to optimum formation of a well-defined vortex street occurs at $f_e/f_0^* = 1.35$, well above the expected value of $f_e/f_0 \sim 1$. The increase in coherence of the downstream wake in this photo is accompanied by vortex formation closer to the base of the cylinder.

Figure 5 further clarifies the flow structure in the very near-wake region as a function of excitation frequency. These close-up photos are phase-locked at the instant of maximum positive displacement of the cylinder, as opposed to the maximum negative displacement condition shown in the previous series. For frequency ratio f_e/f_0^* up to 1.75, there are two simultaneous tendencies: movement of the separation surface upstream towards the base of the cylinder, eventually reattaching to the bottom right corner of it; and movement of the initially formed large-scale vortex of clockwise sense towards the base of the cylinder. At $f_e/f_0^* = 2.2$, the large-scale vortex pattern in the wake breaks into a new mode (compare with figure 4). At $f_e/f_0^* = 3$, there is an additional elongated vortex of opposite sense formed between two vortices of like sense from the bottom portion of the cylinder. This trend continues at $f_e/f_0^* = 4.4$ with production of a counter-rotating vortex pair between the two small-scale vortices on the lower side.

4.4. *Phase of arrival of vortical wave in the near wake*

To quantitatively characterize the phase of the vortex shedding shown in figures 2–5 relative to the cylinder motion, $\Delta\phi_v = \phi_v - \phi_y$, cross-spectral analysis was carried out. Data were from the hot-film signal indicating the fluctuating velocity and the displacement transducer of the forcing mechanism. The hot film was located at $x/D = 1$ and $y/D = 3$, in accord with the phase-gradient criterion described in §2. Figure 6(*a*) shows $\Delta\phi_v$ as a function of f_e/f_0^* for the circular cylinder. In general, at frequencies below synchronization, $f_e/f_0^* < 1$, there is an increase in $\Delta\phi_v$ with increasing f_e/f_0^*. The jump at synchronization, $f_e/f_0 \approx 1$, is approximately π; further increases in frequency above this value result in only mild changes in $\Delta\phi_v$. There is nearly coincidence of the phase data for the three Reynolds numbers considered, $Re_D = 584$, 855 and 1138. In fact, experiments up to $Re_D = 3030$, the highest value attainable with the present system, also showed a well-defined change in $\Delta\phi_v \approx \pi$ near or at $f_e/f_0^* = 1$.

We next address the phase shift $\Delta\phi_v$ as a function of excitation frequency f_e/f_0^* for

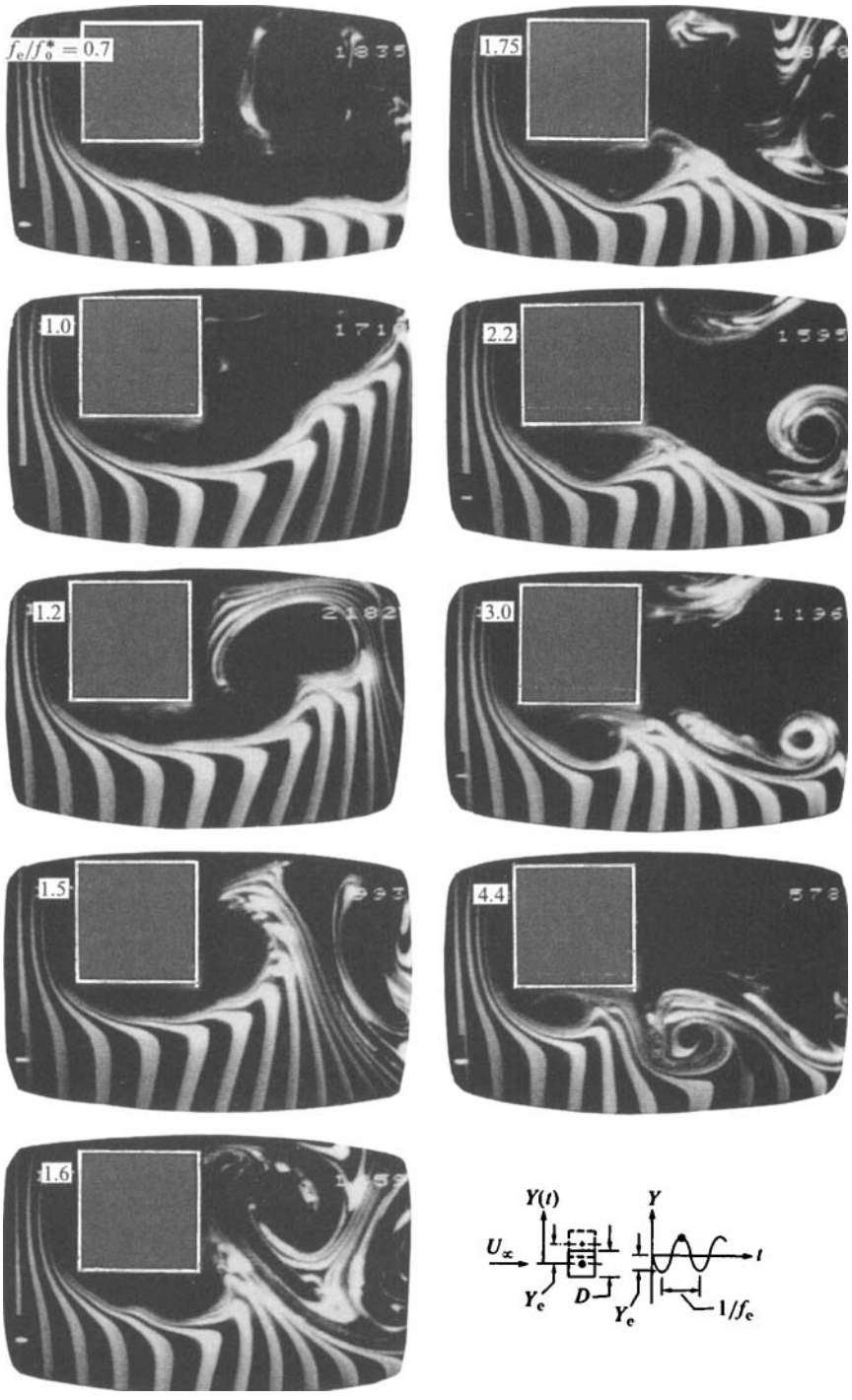

FIGURE 5. Close-up of flow structure on lower side of square cylinder as function of frequency ratio f_e/f_0^*. All photos taken at instant when cylinder displacement is at its maximum positive location.

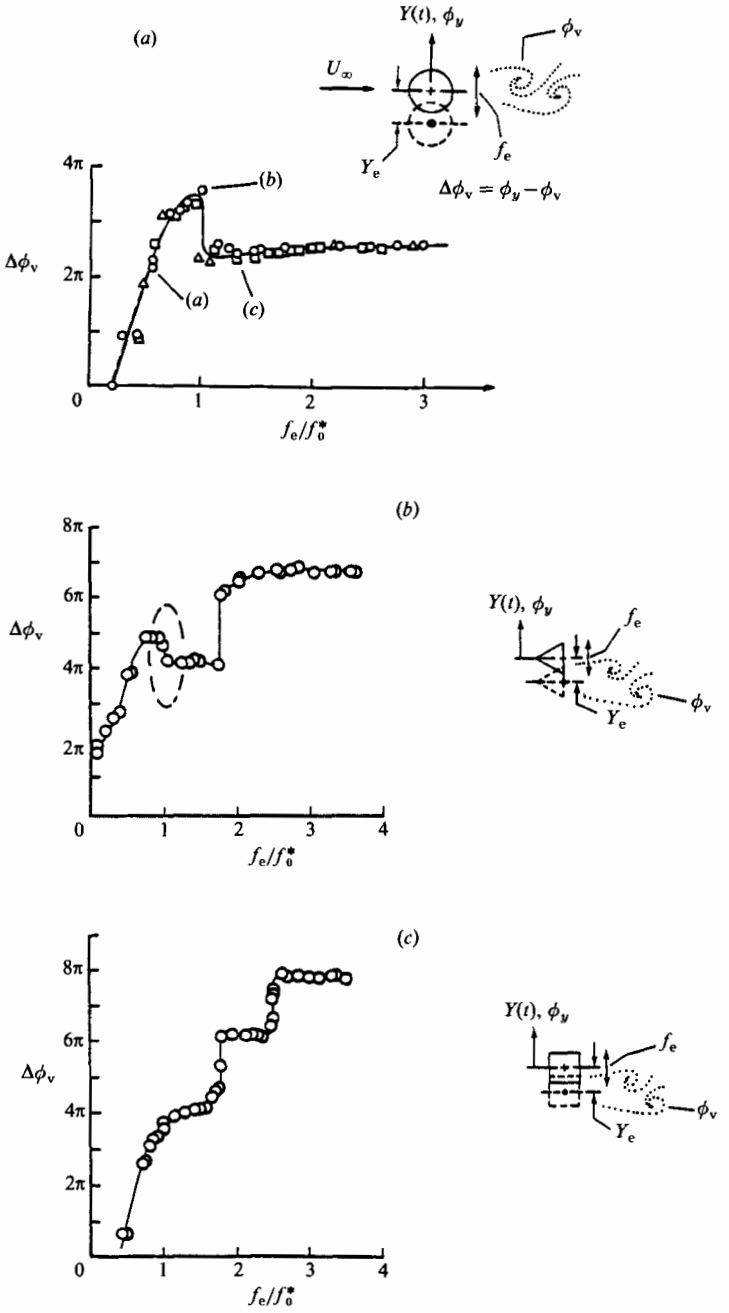

FIGURE 6. Phase $\Delta\phi_v$, representing phase of vortex arrival ϕ_v relative to phase of body displacement ϕ_y, as function of frequency ratio f_e/f_0^* for (*a*) circular-, (*b*) triangular- and (*c*) square-cross-section cylinders. □, $Re_D = 1138$; ○, 855; △, 584.

triangular- and square-cross-section cylinders shown in figure 6(*b* and *c*). In the case of the triangular cylinder, the variation of phase is remarkably similar to that of the circular cylinder. The additional phase jump of $\sim 2\pi$ at $f_e/f_0^* \approx 2$ is due to the abrupt decrease in wavelength of the vortex street (see photo for $f_e/f_0^* = 2.25$ in figure 3).

On the other hand, the square-cross-section cylinder does not show a phase jump

within the range $f_e/f_0^* \sim 1$. Remarkable, however, is the abrupt change of $\Delta\phi_v$ at $f_e/f_0^* = 1.75$ and 2.5. As described in detail by Ongoren (1986), there is a drastic change in wavelength of the vortices, decreasing from $1.67D$ to $0.87D$, in going from excitation frequency $f_e/f_0^* = 1.8$ to 2.25. This halving of the wavelength would correspond to a phase change of 2π, measured by the hot film in the near-wake region; indeed, the phase jump in figure 6 has a value of about 2π. Concerning the second phase jump, occurring in figure 6 at $f_e/f_0^* \approx 2.5$, it corresponds to formation of an additional, elongated vortex at $f_e/f_0^* = 3$, relative to the case of $f_e/f_0^* = 2.2$. This additional vortex is shed from the base of the cylinder, and therefore has opposite sense relative to its neighbours.

5. Recovery of the vortex street: classes of vortex–vortex interaction

We now address the issue of whether, and how, the disturbed near wake recovers to the large-scale arrangement of the classical vortex street, based on observations over a wide range of frequency and amplitude. In doing so, we examine the near-wake vortex–vortex interactions, then the frequency of the downstream wake resulting from these interactions. Very similar near-wake structure was observed for the circular and triangular cylinders; we show here results for the latter, in view of their clarity. (Further results are given by Ongoren 1986.)

5.1. *Vortex interactions at sub-, super-, and non-harmonic excitation*

Figure 7(*a*) gives an overview of the primary characteristics of vortex interactions leading to the recovered f_0 vortices. Subharmonic excitation at $f_e/f_0^* = 0.5$ induces a row of alternating vortices that eventually relaxes to a street of vortices at f_0. This vortex street has, at least in this initial region of formation, small transverse spacing; in addition, there is clearly a lack of coherence of the induced vortices. At $f_e/f_0^* = 1$, there is a dramatic increase in both transverse spacing and coherence of the vortices. A further increase in frequency to the case of non-harmonic excitation at $f_e/f_0^* = 1.5$ produces a remarkable interaction of vortices of like and unlike sense. As indicated in the schematic, there is simultaneous coalescence of three vortices; two of them have like sense and one has an unlike sense of circulation. These three vortices form a large-scale recovered vortex at frequency f_0. In fact, each recovered vortex shows this same pattern of interaction; the vortex patterns leading to recovery are phase-locked to the motion of the cylinder. (At sufficiently low amplitude, this adjustment process to the recovered vortex at f_0, arising from non-harmonic excitation, is somewhat different as described by Ongoren 1986.)

Figure 7(*b*) shows superharmonic excitation at $f_e/f_0^* = 2$, 3 and 4. At $f_e/f_0^* = 2$, two externally induced vortices at f_e coalesce to form the recovered f_0 vortex on each side of the vortex street; of course, this process of vortex coalescence and recovery occurs approximately π out-of-phase between the upper and lower portions of the wake. At $f_e/f_0^* = 3$, there is first coalescence of two adjacent f_e vortices; in turn, these coalesced vortices interact with a single f_e vortex to produce a recovered vortex at f_0 which is comprised of three f_e vortices. In the case of $f_e/f_0^* = 4$, there is again coalescence with two additional f_e vortices, giving a recovered vortex of f_0 embodying four f_e vortices.

These patterns of vortex coalescence occurring at superharmonic frequencies, $f_e/f_0^* = n = 2$, 3 and 4, exhibit the following generalized behaviour. The first vortex coalescence on each side of the wake involves two small-scale vortices; subsequently, these coalesced vortices interact with $n-2$ vortices to produce the recovered vortex

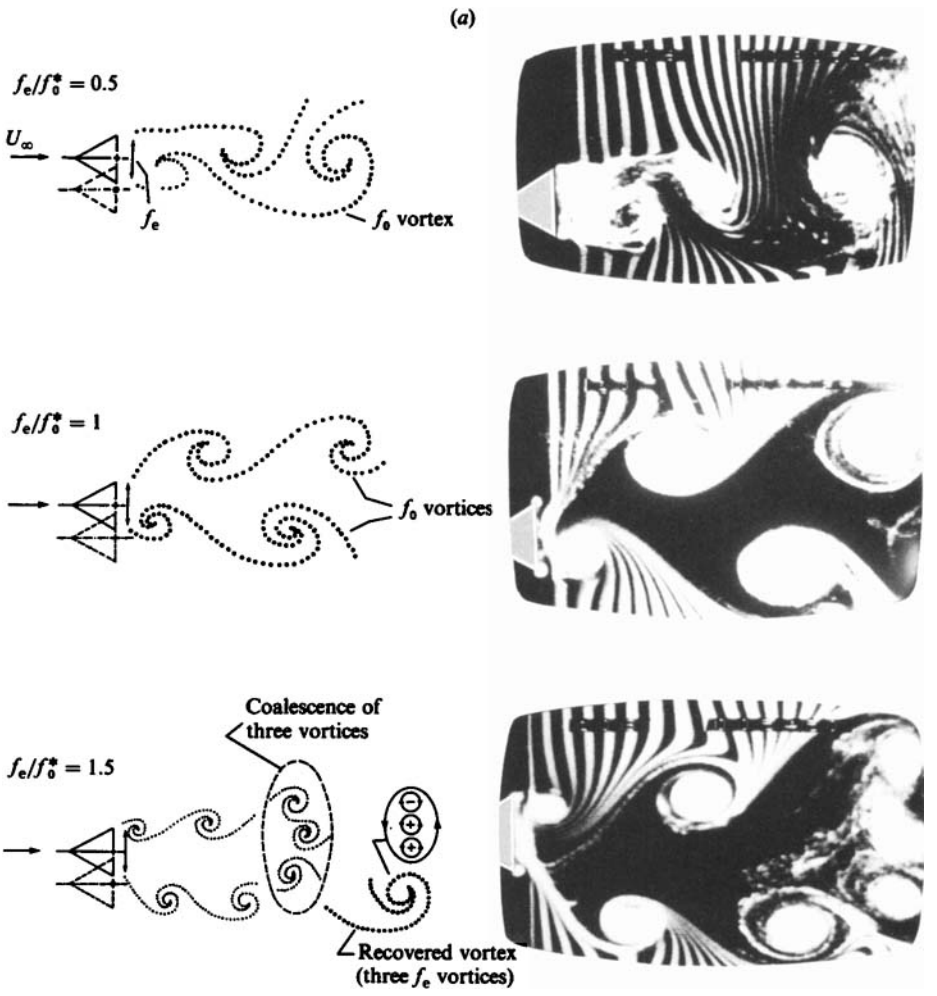

FIGURE 7(*a*). For caption see facing page.

at frequency f_0. These highly ordered and persistent mechanisms of interaction are probably attributable to simultaneous forcing by the oscillating body at f_e and upstream influence at f_0.

Further details of these vortex–vortex interactions are indicated in the time-sequences of figures 8, 9 and 10. Figure 8 represents the non-harmonic excitation at $f_e/f_0^* = 1.5$; it shows, in photo (*i*), the vertical stack of three small-scale vortices with the top two having the same sense, the bottom vortex having opposite sense. The vortex interactions leading to the pattern of photo (*i*) are evident in the right-hand portions of photos (*g*) and (*h*). Subsequently, the stack of three vortices in photo (*i*) is swept away as an f_0 vortex having a sense in the clockwise direction. These patterns of interaction during the oscillation cycle are indeed remarkably ordered and repetitive. At $f_e/f_0^* = 2$ and 4, shown in figures 9 and 10, the interactions leading to recovery of the large-scale vortices at f_0 are again shown to be highly ordered. The patterns repeat in the upper and lower regions of the wake in a π out-of-phase fashion.

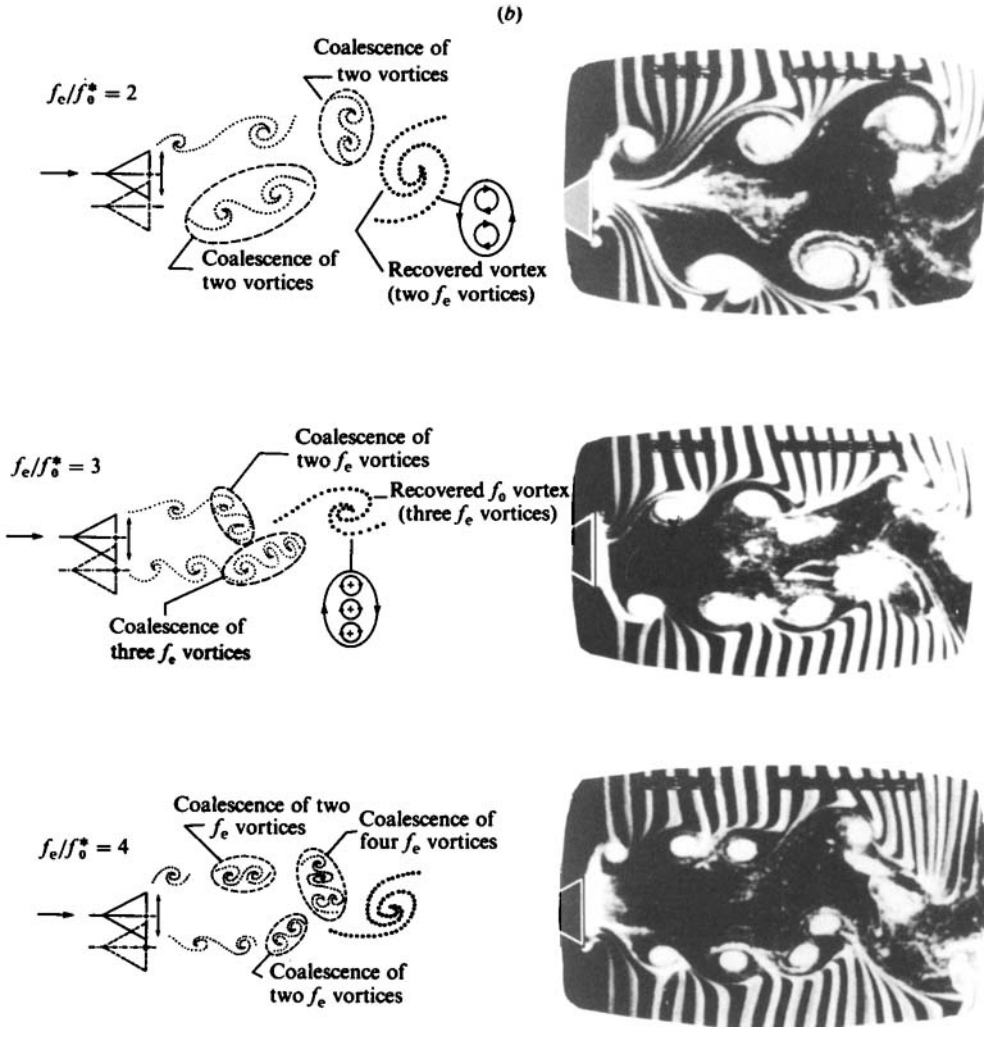

FIGURE 7. (*a*) Schematics and corresponding photos showing mechanisms of recovery of vortices at f_0 due to interaction of vortices generated at f_e for $f_e/f_0^* = 0.5, 1, 1.5$. $Y_e/D = 0.30$. (*b*) Schematics and corresponding photos showing principal mechanisms of recovery of vortices at f_0 due to interaction of vortices generated at f_e for $f_e/f_0^* = 2(Y_e/D = 0.3)$, $3(Y_e/D = 0.13)$ and $4(Y_e/D = 0.13)$.

5.2. *Generalization of vortex–vortex interactions*

On the basis of the extensive flow visualization of the near-wake structure from circular- and triangular-cross-section cylinders subjected to controlled perturbations, it is possible to arrive at a general description of the mechanisms leading to recovery of vortices at f_0. Figure 11 provides an overview of the vortex interactions. In all cases, vortices are initially induced at f_e, and eventually recover to large-scale vortices at f_0. The terminology $+1$, -1, $+2\ldots$ indicates respectively a vortex with counterclockwise sense, a vortex with clockwise sense, two coalesced vortices with counterclockwise sense, etc.

For the case of subharmonic excitation $f_e/f_0^* = 0.5$, the instability at f_e forms an

FIGURE 8. Mechanisms of small-scale vortex–vortex interaction for case of non-harmonic excitation at $f_e/f_0^* = 1.5$. $Re_D = 855$; $Y_e/D = 0.30$.

FIGURE 9. Mechanisms of small-scale vortex–vortex interaction for case of superharmonic excitation at $f_e/f_0^* = 2$. $Y_e/D = 0.30$.

FIGURE 10. Mechanisms of small-scale vortex–vortex interaction for case of superharmonic excitation at $f_e/f_0^* = 4$. $Re_D = 855$; $Y_e/D = 0.13$.

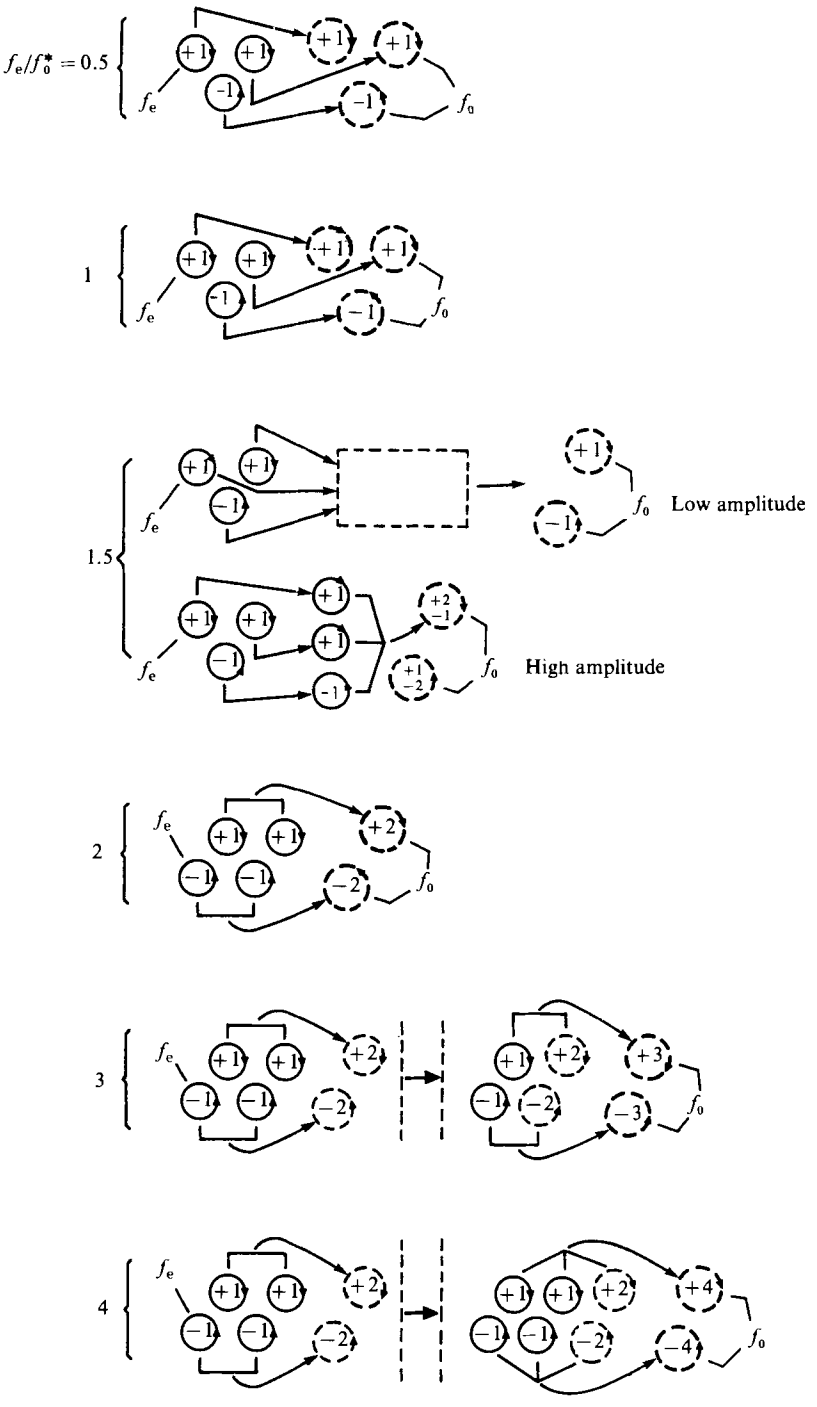

FIGURE 11. Overview of vortex interaction mechanisms where vortices are initially produced at f_e, leading to recovery of large-scale vortices at f_0 for excitation frequencies $f_e/f_0^* = 0.5$, 1, 1.5, 2, 3 and 4. Terminology +1 denotes single vortex in clockwise direction, +2 represents two coalesced vortices in clockwise direction and so on.

f_0 vortex immediately behind the cylinder. The vortices have a long formation length and are phase-locked with the body motion.

At $f_e/f_0^* = 1$, the f_e vortices induced immediately behind the body become the f_0 recovered vortices. We note, however, that the wavelength λ_e between the initially shed vortices may be substantially different than λ_0 of the recovered vortex array; this is due to the variation in phase speed of the induced vortices.

At non-harmonic excitation indicated by $f_e/f_0^* = 1.5$, the f_e vortices tend to be shed nearly symmetrically at an instant during the oscillation cycle if the amplitude is sufficiently small. This process is followed by a collapse in coherence of the near-wake structure and recovery of the large-scale vortices at f_0. During this entire process, there is no coalescence of vortices. On the other hand, for non-harmonic excitation at higher amplitude, there is coalescence of two vortices of like sense and one vortex of unlike sense to produce the recovered f_0 vortices. There appears to be a threshold value of excitation amplitude, above which an excess f_e vortex is produced in the very near wake, necessitating this type of complex coalescence.

At superharmonic excitation corresponding to $f_e/f_0^* = n = 2, 3, 4$, the mechanisms of small-scale vortex interactions are relatively independent of amplitude. In all cases, there is initially coalescence of two small-scale vortices of like sense on either side of the wake. The first stage of the vortex interaction is essentially identical, irrespective of the value of n. In the second phase, there is coalescence of the vortex resulting from the first phase with $n-2$ small-scale vortices at f_e to produce the recovered vortices at f_0.

6. Resonant frequencies of the recovered wake

The foregoing flow visualization shows rapid recovery to large-scale vortex formation at frequency f_0, and the implication is that this frequency approximates the frequency f_0^* of the classical vortex street from a stationary cylinder. However, there are systematic departures from f_0^*. We address this aspect for both triangular and circular cylinders, focusing first on the former, then on the latter.

Figure 12 shows the ratio of the recovered, large-scale vortex frequency f_0 in the presence of (triangular) cylinder excitation to frequency f_0^* in the absence of excitation. (The probe was located at the edge of the mean shear layer where $u/U_e = 0.995$.) The ratio f_0/f_0^* is plotted as a function of f_e/f_0^*, the ratio of the excitation frequency to the natural (unexcited) frequency of the Kármán vortices. Note that the component f_0 is indicated by black dots. Also appearing are relatively large-amplitude components that we designate as interaction components f_0'; they are indicated by the circles.

Remarkable is the substantial departure of f_0/f_0^* from unity, not only in the vicinity of $f_e/f_0^* = 1$, but also for much higher values. In fact, the variation of f_0/f_0^* with f_e/f_0^* clearly exhibits a 'resonant'-type behaviour. That is, f_0/f_0^* tends to follow one of the resonance curves $f_0/f_e^* = 1$, 1/1.5, 1/2, 1/3 and 1/4. This type of resonant response has been well-established in the immediate vicinity of $f_e/f_0^* = 1$ where vortex–vortex interactions do not occur (Staubli 1981; Sarpkaya 1978). Particularly remarkable is the occurrence of this resonant response for the multiplicity of modes shown in figure 12. At this point, we hypothesize that the small-scale, vortex–vortex interactions induced in the near-wake region occur in such a fashion as to maintain synchronization in a given resonant mode over a relatively wide range of excitation frequency f_e/f_0^*; this synchronized behaviour

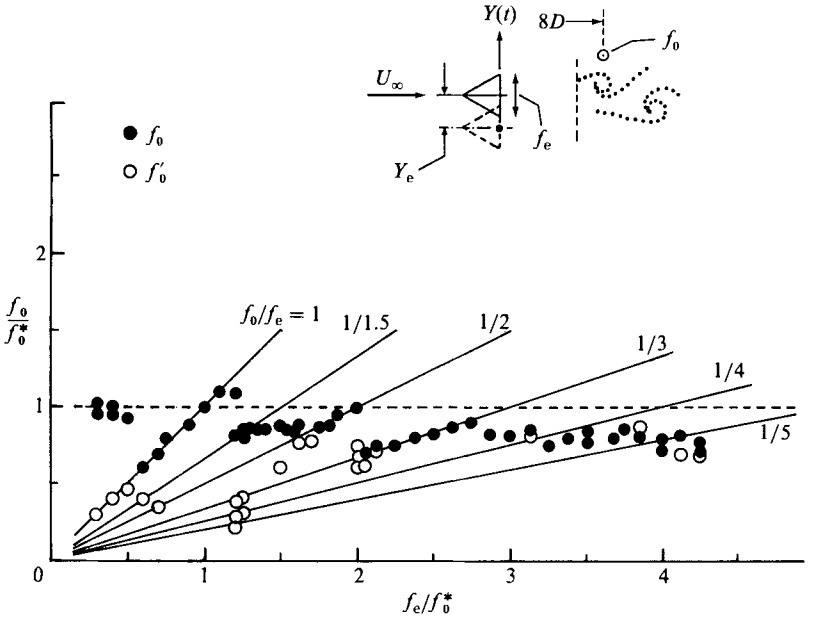

FIGURE 12. Frequency of recovered vortex f_0 and interaction component f_0' relative to frequency f_0^* of vortex formation from corresponding stationary cylinder as function of dimensionless excitation frequency f_e/f_0^*. ($Y_e/D = 0.13$.)

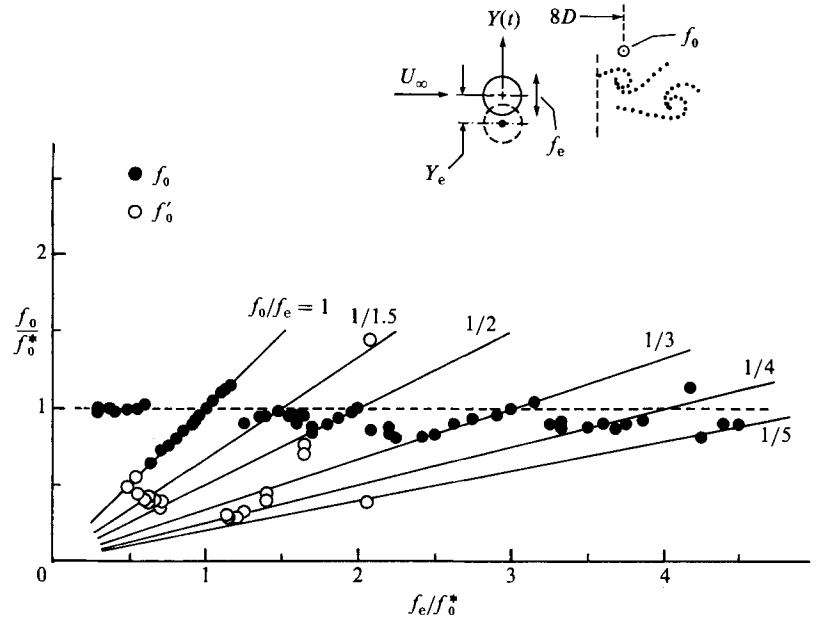

FIGURE 13. Frequency of recovered vortex f_0 and interaction component f_0' relative to frequency f_0^* of vortex formation from corresponding stationary cylinder as function of dimensionless excitation frequency f_e/f_0^*. ($Y_e/D = 0.13$.)

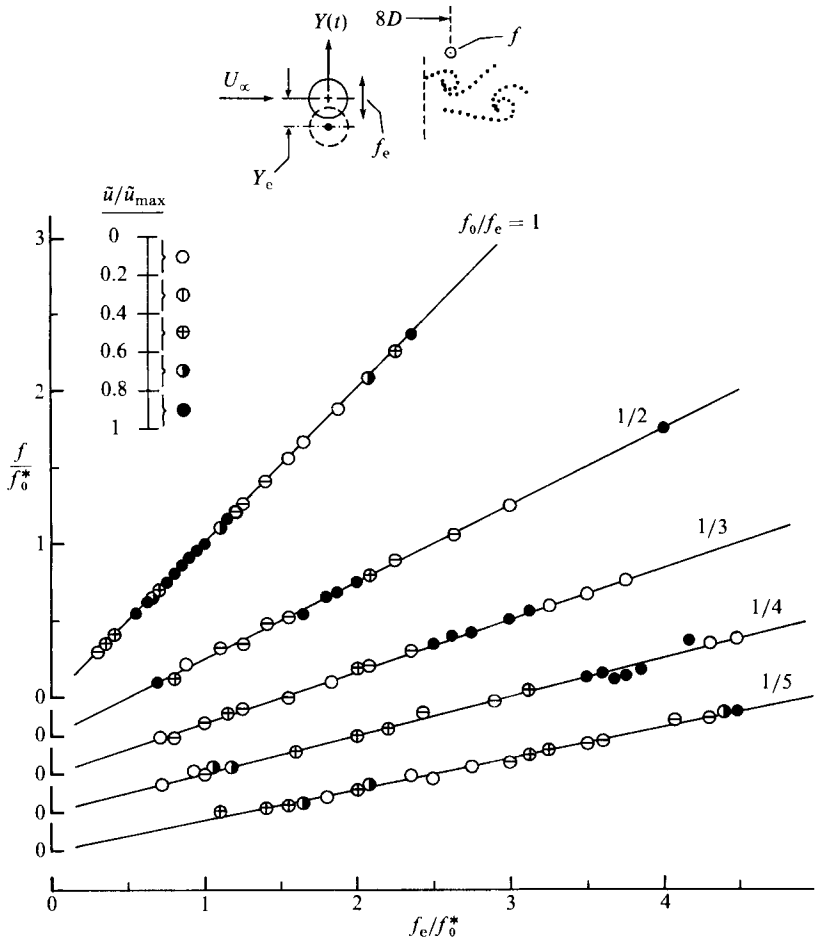

FIGURE 14. Detectable spectral components f relative to recovered vortex frequency f_0 as function of dimensionless excitation frequency f_e/f_0^*. Symbols defined in inset represent the amplitude of the near-wake velocity fluctuation relative to the maximum amplitude $\tilde{u}/\tilde{u}_{max} = 1$.

occurs in conjunction with substantial upstream influence, promoting the mode-locking phenomenon.

In addition to the spectral component f_0, there are a number of other components f_0' present in the wake; at the edge of the mean shear layer some of them have amplitudes commensurate with those of the f_0 component. We term these components as interaction components f_0' in that their value corresponds to a difference frequency between components $f_0/f_0^* = 1$ and $f_0/f_e = 1$, 1/1.5 and 1/2. These differences are indicated by the open circle symbols in figure 12. These interaction components tend to occur at the transition from one mode of resonance, or synchronization, to another.

Figure 13 shows the frequency of the recovered vortices at f_0 for the wake from the circular-cross-section cylinder. These values of f_0 follow the resonant modes given by $f_0/f_e = 1$, 1/1.5, 1/3 and 1/4 in a manner very similar to the flow structure from the triangular cylinder. Moreover, as for the case of the triangular cylinder, the interaction component f_0' indicated by open circle symbols represents the difference frequency between two of the resonant modes.

To further detail the spectral content of the recovered wake, figure 14 shows the frequency of the large-scale vortices f_0 as well as the other, detectable spectral components that are coincident with the resonant modes already defined in figure 13. At a given value of f_e/f_0^*, there are as many as four discrete components. Clearly, nonlinear interaction, which is known to be associated with a number of sum and difference frequencies (Miksad 1972), plays an important role in recovery of the large-scale vortices at f_0.

We note that the resonant response shown in figures 12 and 13 is analogous to the frequency-locking occurring in incompressible, unstable shear layers having finite lengthscale in the streamwise direction, i.e. impinging shear layers (Rockwell 1983). Moreover, this resonant response has a similar form as free-shear (e.g. jet) flows coupled with acoustic resonance modes of a pipe (Kibens 1980). These observations suggest, for the flow therein, the presence of a controlling mechanism in conjunction with the developing instability of the separating shear layer.

That such a controlling mechanism is present is further suggested by the variations of kinetic energy of the shear layer with streamwise distance (Ongoren 1986). Energy at recovered spectral component f_0 rapidly dominates, irrespective of the excitation frequency f_e.

7. Concluding remarks

Synchronization, whereby the vortex formation is phase-locked to the cylinder motion, can take two basic forms. The first is subharmonic synchronization; in this case, the initially formed vortex is always from the same side of the body, irrespective of whether it moves towards its extreme positive or negative position. The second is fundamental synchronization; it is the classical type, involving successive vortex shedding from either side of the body, as it alternately moves towards its maximum negative and maximum positive positions during an oscillation cycle. The fact that both subharmonic and fundamental synchronization can occur has important implications for the general class of problems involving vortex shedding from oscillating bodies. That is, there is more than one admissible phase relation between body motion and shedding of vorticity that gives phase-locking, or synchronization. For example, successive downward and upward movement of the body can be associated with shedding of vortices of either the same or opposite sense, depending upon whether there is subharmonic or fundamental synchronization.

The phase of the initial vortex formation, relative to the body displacement, can undergo drastic changes in the region where the frequency of body excitation approximates that of the natural vortex shedding. For cylinders having a short or zero afterbody length, such as the circular- or triangular-cross-section cylinder, there is a phase switch of the initially shed vortex from the upper to the lower side of the cylinder or vice versa. This switch occurs over a narrowly defined range of excitation frequency. A necessary condition for the switch to occur is attainment of a minimum of the vortex formation length. This phase switch occurs for bodies having both oscillating and fixed separation points; however, the direction of the switch is opposite for the circular-, as compared to the triangular-, cross-section cylinder. This sensitivity to afterbody shape suggests that a global criterion accounting for the flow dynamics in the base region must be accounted for in describing the mechanism of phase switch.

This switch in phase of the initially formed vortex can be prevented altogether if the cylinder has significant afterbody length. As an illustration, we have considered

the case of the square-cross-section cylinder. It precludes a switch through intricate processes of: instantaneous reattachment to a side of the cylinder; and upstream migration of the initially formed large-scale vortex towards the base of the body. We note, however, that the measurements of Bearman & Obasaju (1982) at a higher Reynolds number show a phase shift between loading on, and displacement of, the square cylinder. Further studies are required to relate the detailed nature of the surface pressure to the instantaneous flow structure, and the degree to which it is Reynolds-number dependent.

For all cylinder cross-sections examined, there exists a threshold value of body oscillation frequency above which the near-wake structure breaks into a new mode, characterized by smaller vortices of much shorter wavelength. This threshold frequency depends strongly upon the cross-section of the body, and whether or not the separation points are fixed. In some cases, this small-scale vortex formation actually can retard the onset of large-scale vortex formation in the downstream region of the wake.

For all cylinder cross-sections examined, there exists a threshold value of body oscillation frequency above which the near-wake structure breaks into a new mode, characterized by smaller vortices of much shorter wavelength. This threshold frequency depends strongly upon the cross-section of the body, and whether or not the separation points are fixed. In some cases, this small-scale vortex formation actually can retard the onset of large-scale vortex formation in the downstream region of the wake.

For a cylinder having oscillating separation points, i.e. a circular cylinder, an additional phenomenon is present at frequencies below the natural vortex-shedding frequency. The entire base region of the cylinder undergoes a large-amplitude swinging motion, reaching its maximum angle of swing when the body excitation frequency equals that of the naturally shed vortices. Then, at higher excitation frequency the magnitude of this base swing angle abruptly drops. In fact, this swinging effect is well correlated with the switch in phasing of the initially shed vortex described in the foregoing. For bodies having fixed separation points, there is no such base-swinging mechanism; yet, as noted in the foregoing, a switch in phase of the initially shed vortex is still an admissible process. These phenomena of phase switch of the initially formed vortex and swinging of the base region are intertwined with the rapid increase, then abrupt loss, of fluctuating lift.

In addition to the foregoing aspects of synchronization and phase shift, we have addressed the time-dependent development of the large-scale vortex street from the nonlinearly distorted near wake. Over a wide range of excitation conditions, there is consistently recovery of the near wake to the preferred, or Kármán, mode. Moreover, we have observed that the frequency f_0 of the recovered vortex street can depart substantially from that of the natural vortex-shedding frequency f_0^*. In fact, this frequency f_0 shows a resonant-type response, reminiscent of resonant modes occurring in incompressible systems having finite streamwise lengthscale (Rockwell 1983), as well as those arising from coupling between shear-layer instabilities and organ-pipe modes of the flow system (Kibens 1980). Of course, the free wake falls in neither of these categories. It is a purely hydrodynamic system having infinite streamwise lengthscale.

This recovery of the large-scale vortices and resonant response of the f_0 component occur under two important influences: a strongly non-parallel shear-layer development from initial separation of the thin shear layers to where the wake fills in; and upstream influence from the downstream wake dynamics. We suggest that this

excitation from the upstream influence, in conjunction with the non-parallel shear-layer development, is substantial enough to promote the rapid and repetitive vortex–vortex interactions leading to recovery of the large-scale vortices having the same frequency f_0 as the predominant upstream influence. As yet, it is unresolved to what degree this upstream influence arises from Biot–Savart induction from the large-scale vortices in the downstream region of the wake, and to what degree it arises from upstream wave reflection due to the existence of an absolute instability. It is instructive to address in further detail the nature of this upstream influence in the bluff-body wake in relation to the instabilities occurring in typical jets and mixing layers. We now focus on this aspect.

As a basis for examining perturbed bluff-body wakes, we have available an extensive foundation from studies of mixing layers and jets (Ho & Huerre 1984). Although, as will be demonstrated, there are some marked differences between instabilities associated with these classes of flows and those of bluff-body wakes, certain features are indeed relevant. An advance of central importance is the recognition of successive coalescence of vortices that increase the scale and decrease the frequency of the shear-layer unsteadiness (Winant & Browand 1974; Brown & Roshko 1974; Roshko 1976). To be sure, there are a wide range of mechanisms of successive vortex coalescence associated with phase and amplitude modulation of the evolving shear layer. When the mixing layer is excited at a frequency f_e sufficiently close to the inherent instability frequency f_0 (i.e. most unstable frequency) of the shear layer, then the instability synchronizes with the external excitation. Further downstream, however, subharmonic(s) of f_e, arising from vortex coalescence become dominant (Miksad 1972; Ho & Huang 1982). Furthermore, if the mixing-layer or jet is excited with sufficiently high amplitude at one of its subharmonics (Ho & Huang 1982; Rockwell 1972), then there occurs 'forced fusion' or 'collective coalescence' of a number of small-scale vortices originally formed at the inherent instability frequency f_0. If the forcing frequency is of the order of one-tenth of the inherent instability frequency f_0, then a large number of small-scale vortices at f_0 roll into the large-scale vortices at frequency f_e. If, at the other extreme, the separating shear layer is excited at a frequency f_e significantly higher than its inherent instability frequency f_0, then it is actually possible to retard the growth of the vortex formation associated with the primary instability at f_0 (Rockwell 1972). Certain of these elements are, to a degree, evident in the bluff-body wake configuration herein.

In general, these vortex interactions must be considered in conjunction with the downstream regions of the flow. It has been recognized recently that upstream influence from the downstream vorticity dynamics may, in turn, influence the initial evolution of the instability from the trailing edge onwards (Rockwell 1983; Ho & Huerre 1984). In fact, Michalke (1984) suggests that the initial instability is controlled by the downstream vorticity dynamics. For this reason, the self-excited instability frequency f_0 is substantially lower than that predicted from linear stability theory. Dimotakis & Brown (1976), taking the view of the flow field as a whole, point out that even regions well downstream of the trailing edge can exert a substantial upstream influence. More recently, Laufer & Monkewitz (1980) address in detail the consequence of the sudden change in circulation during vortex coalescence on the upstream influence; with this concept in view, Ho & Nossier (1981) propose a simple relation for the location of the vortex merging (or coalescence).

Characterization of upstream influence in bluff-body wakes has received far less attention. Particularly striking are the high fluctuation levels in the separation region of a cylinder, as well as the formation of large-scale vortices close to the

cylinder over certain ranges of Reynolds number (Unal & Rockwell 1988). Biot–Savart induction from the downstream vorticity dynamics will always, to varying degrees, exert an influence on the initially developing instability. However, the possible existence of a region of local absolute instability, which occurs at a streamwise location after the initially thin mixing layers have filled in to form a wake-type profile (Koch 1984; Huerre & Monkewitz 1985; Monkewitz & Nguyen 1986), may exert the predominant influence. Since the group velocity goes to zero at the location of the local absolute instability, there can actually be a reflection of energy at this location; this upstream reflection can, in turn, excite the initially growing instability. In other words, there may be a self-sustaining feedback loop in the near wake.

The authors are pleased to acknowledge primary financial support of the Office of Naval Research and supplemental support of the Volkswagen Foundation. Dr Thomas Staubli engaged the authors in several helpful discussions during the course of this investigation.

REFERENCES

ANGRILLI, F., DISILVIO, G., ZANARDO, D. 1974 Hydroelasticity study of a circular cylinder in a waterstreak. In *Flow-Induced Structural Vibrations* (ed. E. Naudascher), pp. 504–512. Springer.

BEARMAN, P. W. 1984 Vortex shedding from oscillating bluff bodies. *Ann. Rev. Fluid Mech.* **16**, 195–222.

BEARMAN, P. W. & CURRIE, I. G. 1979 Pressure fluctuation measurements on an oscillating circular cylinder. *J. Fluid Mech.* **91**, 661–677.

BEARMAN, P. W. & GRAHAM, J. M. R. 1980 Vortex shedding from bluff bodies in oscillatory flow: A report on Euromech 119. *J. Fluid Mech.* **99**, 225–245.

BEARMAN, P. W. & OBASAJU, E. D. 1982 An experimental study of pressure fluctuations on fixed and oscillating square-section cylinders. *J. Fluid Mech.* **119**, 297–321.

BERGER, E. & WILLE, R. 1972 Periodic flow phenomena. *Ann. Rev. Fluid Mech.* **24**, 313–340.

BISHOP, R. E. D. & HASSAN, A. Y. 1964 The lift and drag forces on a circular cylinder oscillating in a flowing fluid. *Proc. R. Soc. Lond.* A **227**, 51–75.

BROWN, G. L. & ROSHKO, A. 1974 On density effects and large-scale structure in turbulent mixing layers. *J. Fluid Mech.* **64**, 775–816.

DEN HARTOG, J. P. 1934 The vibration problems of engineering. In *Proc. Fourth Intl Congr. on Applied Mechanics, Cambridge, England*, pp. 36–53.

DIMOTAKIS, P. E. & BROWN, G. L. 1976 The mixing layer at high Reynolds numbers: large-scale dynamics and entrainment. *J. Fluid Mech.* **78**, 535–560.

FENG, C. C. 1968 Measurement of vortex-induced effects in flow past stationary and oscillating circular and D-section cylinders. M.Sc. thesis, University of British Columbia, Vancouver, Canada.

FERGUSON, M. & PARKINSON, G. V. 1967 Surface and wake flow phenomena of the vortex-excited oscillation of the circular cylinder. *Trans. ASME* B: *J. Engng for Industry* **89**, 831–838.

GERRARD, J. H. 1978 The wakes of cylindrical bluff bodies at low Reynolds number. *Phil. Trans. R. Soc. Lond.* A **288**, 351–382.

GRIFFIN, O. M. 1971 The unsteady wake of an oscillating cylinder at low Reynolds number. *Trans. ASME* E: *J. Appl. Mech.* **38**, 729–738.

GRIFFIN, O. M. 1973 Instability in the vortex street wakes of vibrating bluff bodies. *Trans. ASME* I: *J. Fluids Engng* **95**, 569–581.

GRIFFIN, O. M. & VORTEX, C. W. 1972 The vortex street in the wake of a vibrating cylinder. *J. Fluid Mech.* **51**, 31–48.

HO, C. M. & HUANG, L. S. 1982 Subharmonic and vortex merging in mixing layers. *J. Fluid Mech.* **119**, 443–473.

HO, C. M. & HUERRE, P. 1984 Perturbed free-shear layers. *Ann. Rev. Fluid Mech.* **16**, 365–424.

Ho, C. M. & Nossier, N. S. 1981 Dynamics of an impinging jet. Part I. The feedback phenomenon. *J. Fluid Mech.* **105**, 119–142.

Huerre, P. & Monkewitz, P. A. 1985 Absolute and convective instabilities in free-shear layers. *J. Fluid Mech.* **59**, 151–168.

Kibens, V. 1980 Interaction of jet flow field instabilities with flow system resonances. Presented at *AIAA Aeroacoustics Meeting, 5–7 June, Hartford, Connecticut.*

Koch, W. 1984 Local instability characteristics and frequency determination of self-excited wake flows. *J. Sound Vib.* **99**, 53–83.

Koopmann, G. H. 1967*a* The vortex wakes of vibrating cylinders at low Reynolds numbers. *J. Fluid Mech.* **28**, 501–512.

Koopmann, G. H. 1967*b* On the wind-induced vibrations of circular cylinders. M.Sc. thesis, Catholic University of America, Washington, DC.

Laufer, J. & Monkewitz, P. A. 1980 On the turbulent jet flow in a new perspective. *AIAA Paper* 80-0962.

Mair, W. A. & Maull, D. J. 1971 Bluff bodies in vortex shedding – A report on Euromech 17. *J. Fluid Mech.* **45**, 209–224.

Meier-Windhorst, A. 1939 Flatterschwingungen von Zylindern im gleichmässigen Flüssigkeitsström. *Mitteilungen des Hydraulischen Instituts der Technichen Hochschule, Munchen*, Heft 9, pp. 3–39.

Michalke, A. 1965 On spatially growing disturbances in an inviscid shear layer. *J. Fluid Mech.* **23**, 521–544.

Michalke, A. 1984 Survey on jet instability theory. *Prog. Aerospace Sci.* **21**, 159–199.

Miksad, R. W. 1972 Experiments on the nonlinear stages of shear layer transition. *J. Fluid Mech.* **56**, 695–719.

Monkewitz, P. A. & Nguyen, L. N. 1986 Absolute instability in the near-wake of bluff-bodies. *J. Fluids and Structures* **1**, 165–184.

Ongoren, A. 1986 Unsteady structure and control of near-wakes. PhD. dissertation, Department of Mechanical Engineering and Mechanics, Lehigh University, Bethlehem, Pennsylvania.

Parkinson, G. V. 1974 Mathematical models of flow-induced vibrations. In *Flow-Induced Structural Vibrations* (ed. E. Naudascher), pp. 81–127. Springer.

Rockwell, D. 1972 External excitation of planar jets. *Trans. ASME* E: *J. Appl. Mech.* **39**, 883–890.

Rockwell, D. 1983 Invited lecture: Oscillations of impinging shear layers. *AIAA J.* **21**, 645–664.

Roshko, A. 1976 Structure of turbulent shear flows: A new look. *AIAA J.* **14**, 1349–1357.

Sarpkaya, T. 1978 Fluid forces on oscillating cylinders. *J. Waterways, Ports, Coastal Ocean Div., ASCE* **104**, 275–290.

Sarpkaya, T. 1979 Vortex-induced oscillations: A selective review. *Trans. ASME* E: *J. Appl. Mech.* **26**, 241–258.

Schraub, F. A., Kline, S. J., Henry, J., Runstadler, P. W. & Little, A. 1965 Use of hydrogen bubbles for quantitative determination of time-dependent velocity fields in low-speed water flows. *Trans. ASME* D: *J. Basic Engng* **87**, 429–444.

Staubli, T. 1981 Calculation of the vibration of an elastically mounted cylinder using experimental data from a forced oscillation. In *ASME Symp. on Fluid–Structure Interaction in Turbomachinery*, pp. 19–24.

Unal, M. F. & Rockwell, D. 1988 On vortex formation from a cylinder: Part 1 – The initial instability. *J. Fluid Mech.* **190**, 491–512.

Wei, T. & Smith, C. R. 1986 Secondary vortices in the wake of circular cylinders. *J. Fluid Mech.* **169**, 513–533.

Winant, C. D. & Browand, F. K. 1974 Vortex pairing, the mechanism of turbulent mixing layer growth at moderate Reynolds number. *J. Fluid Mech.* **63**, 237–255.

Zdravkovich, M. M. 1982 Modification of vortex shedding in the synchronization range. *Trans. ASME* I: *J. Fluids Engng* **104**, 513–517.